Analyst

Single-Step Bioassays in Serum and Whole Blood with a Smartphone, Quantum Dots and Paper-in-PDMS Chips

Journal:	*Analyst*
Manuscript ID:	AN-ART-03-2015-000475.R1
Article Type:	Paper
Date Submitted by the Author:	16-Apr-2015
Complete List of Authors:	Petryayeva, Eleonora; University of British Columbia, Chemistry Algar, Walter; University of British Columbia, Department of Chemistry

Table of Contents Entry

The optical properties of quantum dots permit single-step bioassays in whole blood using a custom chip and smartphone-based readout platform.

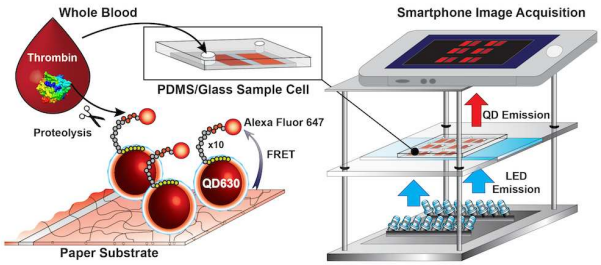

Single-Step Bioassays in Serum and Whole Blood with a Smartphone, Quantum Dots and Paper-in-PDMS Chips

Eleonora Petryayeva and W. Russ Algar*

Department of Chemistry, University of British Columbia, 2036 Main Mall, Vancouver, British Columbia, V6T 1Z1, Canada.

*Corresponding author: algar@chem.ubc.ca

Abstract

The development of nanoparticle-based bioassays is an active and promising area of research, where point-of-care (POC) diagnostics are one of many prospective applications. Unfortunately, the majority of nanoparticle-based assays that have been developed to date have failed to address two important considerations for POC applications: use of instrumentation amenable to POC settings, and measurement of analytes in biological sample matrices such as serum and whole blood. To address these considerations, we present design criteria and demonstrate proof-of-concept for a semiconductor quantum dot (QD)-based assay format that utilizes smartphone readout for the single-step, Förster resonance energy transfer (FRET)-based detection of hydrolase activity in serum and whole blood, using thrombin as a model analyte. Important design criteria for assay development included (i) the size and emission wavelength of the QDs, which had to balance brightness for smartphone imaging, optical transmission through blood samples, and FRET efficiency for signaling; (ii) the wavelength of a light-emitting diode (LED) excitation source, which had to balance transmission through blood and the efficiency of excitation of QDs; and (iii) the use of an array of paper-in-polydimethylsiloxane (PDMS)-on-glass sample chips to reproducibly limit the optical path length through blood to *ca*. 250 μm and permit multiplexing. Ultimately, CdSe/CdS/ZnS QDs with peak emission at 630 nm were conjugated with Alexa Fluor 647-labeled peptide substrates for thrombin and immobilized on paper test strips inside the sample cells. This FRET system was sensitive to thrombin activity, where the recovery of QD emission with hydrolytic loss of FRET permitted kinetic assays in buffer, serum and whole blood. Quantitative results were obtained in less than 30 min with a

limit of detection 18 NIH units mL^{-1} of activity in 12 μL of whole blood. Proof-of-concept for a competitive binding assay was also demonstrated with the same platform. Overall, this work demonstrates that the integration of QDs with smartphones and other consumer electronics can potentiate bioassays that are highly amenable to future point-of-care diagnostic applications.

Keywords: Quantum dot, Förster resonance energy transfer (FRET), proteolysis, blood, serum, imaging, smartphone.

Introduction

Semiconductor quantum dots (QDs) are one of many promising nanoparticles for bioanalysis applications.[1-4] Advantages of these materials include their excellent brightness, broad absorption bands, narrow emission bands that can be spectrally tuned as a function of size and composition, superior resistance to photobleaching, and surface area that is amenable to both chemical and biological functionalization.[5, 6] Although fluorescent dyes and other nanoparticles can sometimes rival QDs in one of these aspects, the cumulative properties of QDs are a rare combination. Consequently, QDs have been widely used as labels for cellular imaging and single biomolecule tracking, encoders for suspension arrays, and probes for biological assays and sensing.[6-11] The latter applications, which include a myriad of Förster resonance energy transfer (FRET) probes, are especially interesting due to the large variety of methods that have been developed and their potential for *in vitro* diagnostics.[12, 13] While an exciting and promising area of research, current limitations of these methods include the frequent use of sophisticated laboratory instrumentation, and infrequent application with clinically relevant biological sample matrices.

In recent years, our group and others have sought to address the foregoing limitations, particularly the need for sophisticated laboratory instrumentation. Smartphones have emerged as promising consumer platforms for the optical readout of assays,[14-18] opening the door to prospective point-of-care diagnostic applications with QDs and other nanoparticles. The Ozcan Laboratory utilized QDs as fluorescent labels in a sandwich immunoassay for the detection of *Escherichia coli* O157:H7 using cell phone imaging,[19] and our group has previously demonstrated the use of smartphone imaging for multiplexed, QD-FRET-based detection of protease activity in solution[20] and with sample application to paper test strips.[21] These examples demonstrate the significant potential of smartphone-based assays with QDs and highlight the need for their continued development. QD-based assays suitable for the direct analysis of analytes in serum matrices have been developed,[22, 23] but represent a small subset of the total assays that have been developed and have required sophisticated instrumentation. Most other serum-compatible assays with QDs also use sophisticated instrumentation and further tend to be heterogeneous formats requiring washing steps.[24-27] Consequently, there is a need for assay

platforms that permit direct, single-step analysis of serum and blood samples, while also utilizing a smartphone or other mass-produced consumer electronic devices for readout.

Here, we outline design criteria and demonstrate proof-of-concept for an assay format that utilizes smartphone readout for the single-step, FRET-based detection of hydrolase activity in serum and whole blood, using thrombin as a model analyte. Thrombin plays a central role in thrombosis and haemostasis, with implications in many diseases including stroke and myocardial infarction based on its procoagulant and anticoagulant functions.[28] Although this study builds on our previous work demonstrating smartphone readout of QD-FRET-based test strips for proteolytic activity[21], a near complete redesign of the assay format was required to permit direct measurements in whole blood. Figure 1 summarizes the new assay format. A sample spot of immobilized QDs, conjugated with an Alexa Fluor 647 (A647)-labeled peptide substrate, responds to thrombin activity through loss of FRET between the QD and A647 with recovery of quenched QD photoluminescence (PL). The reference spot of QD-peptide conjugates is insensitive to thrombin and serves as an internal standard. The paper test strips are placed inside cells in a polydimethylsiloxane (PDMS)-on-glass sample chip, illuminated with an array of blue light-emitting diodes (LEDs), and changes in QD PL are imaged with a smartphone (or other CMOS camera device) to detect thrombin activity. We also show that the test strips can be adapted to a competitive binding FRET-assay format, such that the assay format may have potential utility beyond assays for the activity of proteases or other hydrolases. Each non-smartphone component of this assay format was carefully designed or optimized to enable measurements in whole blood, including the LED illumination, the QD-dye FRET pair, the paper test strips, and the PDMS sample chip. To the best of our knowledge, neither smartphone-based assays with QDs nor QD-FRET assays on other instrument platforms have been demonstrated previously with whole blood samples. Overall, this study shows how consumer electronics and QDs can be integrated to permit assays in serum and whole blood in a format that will ultimately be suitable for many point-of-care diagnostic applications.

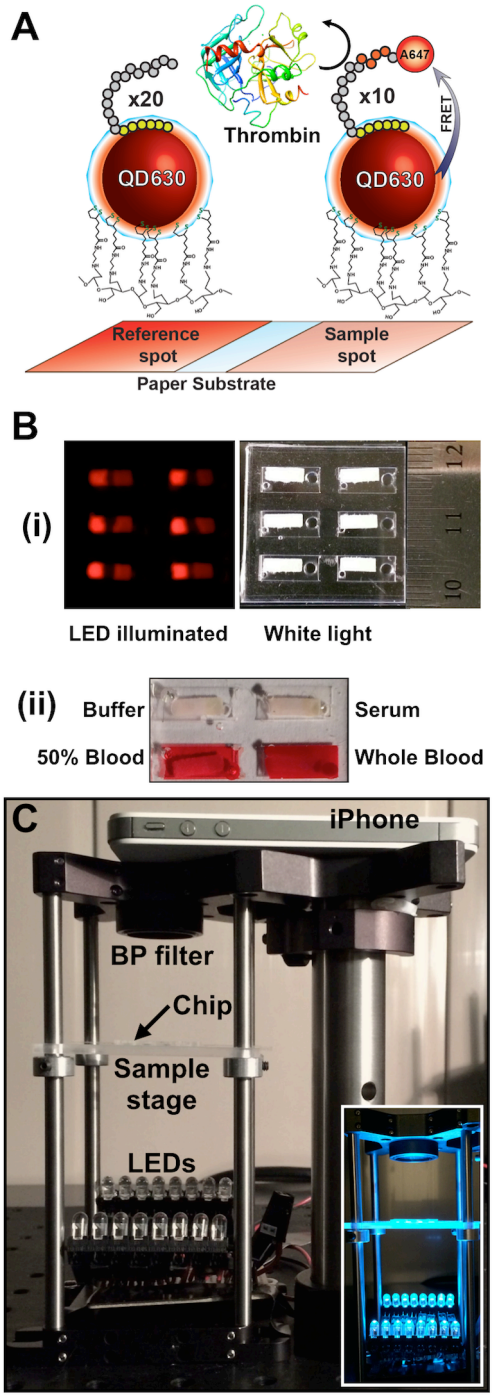

Figure 1. (A) Design of paper test strips to measure thrombin activity *via* FRET with immobilized QD donors and A647 acceptor dye-labeled peptide substrates containing a cleavage site recognized by thrombin. The average number of peptides per QD is indicated (10x, 20x). Protease activity was measured through the recovery QD PL with loss of FRET. **(B)** Paper test strips with sample and reference spots of immobilized QD-peptide conjugates were (i) enclosed within PDMS/glass sample cells that were then (ii) filled with a biological sample matrix such as serum, diluted blood or whole blood. Note the opacity of the whole blood. **(C)** Photograph of the setup used for smartphone readout of QD-FRET test strip assays with serum and blood samples. The inset shows the setup with the LED470 illuminating the PDMS/glass sample chip.

Experimental Section

Detailed experimental methods can be found in the Electronic Supplementary Information (ESI).

Materials

CdSe/CdS/ZnS core/shell/shell QDs with PL emission maxima at 630 nm and 650 nm (QD630 and QD650, respectively) were synthesized using standard methods[29, 30] and made water-soluble by coating with glutathione (GSH) ligands as described previously.[20] A peptide (Bio-Synthesis Inc., Lewisville, TX) with the amino acid sequence H_6SP_6GSDGNESGLVPRGSGC was labeled with Alexa Fluor 647-maleimide (Life Technologies, Carlsbad, CA, USA) as described previously[31] (see SI for details), and is abbreviated as Sub(A647). A second peptide (denoted as Pep throughout the manuscript) was used to prepare QD conjugates for reference spots (*vide infra*). This peptide had the amino acid sequence H_6SP_4SGNLGNDSGWDSGNDSGN and was unlabeled. Human alpha-thrombin was from Haematologic Technologies (Essex Junction, VT, USA), bovine serum (adult) was from Sigma-Aldrich (Oakville, ON, Canada), and defibrinated bovine blood was from Hemostat Laboratories (Dixon, CA, USA).

Preparation of paper substrates

Cellulose filter paper (Whatman, grade 4) was oxidized with 100 mM $NaIO_4$ (*aq*), washed successively with water, methanol, and dichloromethane, dried *in vacuo* overnight, then reacted with *N*-(2-aminoethyl)-5-(1,2-dithiolan-3-yl)pentanamide in dichloromethane, as described previously.[21] The modified paper was further reduced with 50 mM $NaCNBH_3$ (*aq*), washed with water, dried, and stored at –20 °C until needed. Prior to use, the modified paper was cut to the desired size (2 × 6 mm) with a paper punch (Recollections™, Michaels Stores, Inc., Irving, TX, USA). These paper strips were treated with 50 mM $NaBH_4$ (*aq*) for 1–2 h to reduce disulfide groups, and then washed successively with water and ammonium acetate buffer (100 mM, pH 4.5). Excess buffer was removed from the paper substrates with an adsorbent pad, and the substrates were dried in air for 5 min. QD-peptide conjugates were prepared by self-assembly with a 1:10 QD:Sub(A647) ratio at a final QD concentration of 4.0 μM (see SI for details). A 0.5 μL aliquot of QD-Sub(A647) conjugates was directly spotted on one end of the paper substrates. Similarly, reference spots were deposited on the opposite end of paper substrates by

spotting 0.5 μL of QD-Pep conjugate prepared with a 1:20 ratio and at a final QD concentration of 1.0 μM. Substrates were then incubated in a humid chamber for 5–10 min, washed with borate buffer (5 mM, pH 9.2), and dried in the dark.

Enzyme assays and image acquisition

Dilutions of human alpha-thrombin (stock solution: 22000–26000 NIH units mL^{-1} specific activity) were prepared in borate buffer (50 mM, pH 8.5), bovine serum, or bovine blood at final activities between 7.6–480 NIH units mL^{-1}. Proteolytic activity was monitored by adding 12 μL of these thrombin samples to PDMS-on-glass cells containing paper substrates. QD PL was excited using an LED light source (470 nm emission; LED470) and images were acquired at 30 s intervals for 30 min using either (i) an iPhone 5S (Apple, Cupertino, CA) with the Lapse It Pro app (Interactive Universe), or (ii) a USB digital monochrome camera (DCC1545, Thorlabs, NJ, USA) with micro-Manager software.[32] Images were processed using Image J software (NIH, Bethesda, MD, USA). A bandpass filter (624/40; Chroma, Bellows Falls, VT, USA) was placed prior to the detector to block stray LED light. The setup is shown in Figure 1C, and schematics of the chip and detailed methods of image and data analysis are available in the SI.

Results

Assay design: selection of QDs

As noted in the Introduction, several FRET-based assays with QDs have been developed for measuring proteolytic activity and other analytes, but have been rarely utilized with crude samples of biological fluids. Here, the challenge was to adapt the basic QD-FRET assay format to measurements in serum and blood while using low-cost LEDs (≤ $1) and a smartphone or other CMOS camera for readout. It was important to use a readout format that was amenable to point-of-care settings, as that is where crude biological fluids are most likely to be assayed. As shown in Figure 2, blood exhibits strong absorption and scattering across most of the UV-visible spectrum, with the greatest optical transmission in the red and near-infrared (NIR) regions of the spectrum. For this reason, and recognizing that smartphones and most other consumer CMOS devices contain a built-in IR-blocking filter, we evaluated CdSe/CdS/ZnS QDs with red emission for assaying proteolytic activity in serum and blood.

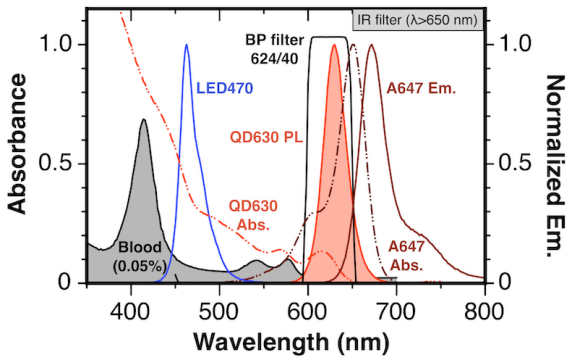

Figure 2. Spectra showing the absorption of a blood sample, the absorption (dashed line) and emission (solid line) spectra associated with the QD630-A647 FRET pair, and the emission spectrum of the LED470 excitation source. The fluorescence spectra are normalized for easy comparison. The absorbance spectra were measured for the following solutions: 0.27 μM QD630, 4.0 μM A647, and 0.05% v/v blood (1 cm path length). The transmission spectrum of a 624/40 bandpass filter used to isolate QD emission prior to the smartphone camera is also shown.

As shown in Figure 3A, two candidate QDs had emission centered at 630 nm (QD630) and 650 nm (QD650). It was necessary to consider their excitation, emission, and FRET signaling properties. The emission intensities from QD630 and QD650 spiked into serum and blood at equal concentrations were first compared, as a function of excitation wavelength, to those in a simple buffer solution, using a monochromator-based fluorescence plate reader. Figure 3B shows that the QD emission intensities decreased by *ca*. 15–45% in serum and by *ca*. 82–98% in whole blood. The QD630 and QD650 had quantum yields of 0.77 and 0.25, respectively; however, the larger molar absorption coefficient of QD650 (dashed lines, Figure 3B) led to better overall brightness, and the longer emission wavelength of the QD650 provided slightly better retention of signal in serum and blood for excitation wavelengths between 350–570 nm. In buffer samples, a 1.4-fold higher signal was observed from the QD650 *via* smartphone imaging with optimized bandpass filters (624/40 and 650/40 for QD630 and QD650, respectively, where the numbers indicate the center wavelength/bandwidth for transmission). The impact of the built-in IR filter associated with the smartphone camera was evident as the QD650 was 2.8-fold brighter than the QD630 when measured with a fluorescence plate reader.

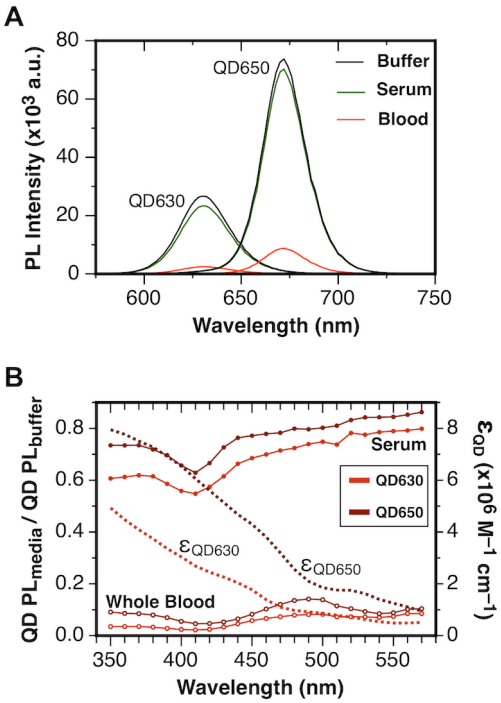

Figure 3. (A) Variation in the intensity of the QD630 and QD650 PL spectra as a function of sample matrix (excitation at 470 nm). **(B)** Excitation wavelength-dependent attenuation of the QD630 and QD650 PL in serum and whole blood (solid lines). The wavelength-dependent molar absorption coefficients of QD630 and QD650 are also shown (dashed lines). These measurements were done with a fluorescence plate reader.

In addition to brightness, another important consideration was FRET for signaling proteolysis. We paired QD630 with Alexa Fluor 647 (A647) and QD650 with Alexa Fluor 680 (A680). The absorption and emission spectra, and the spectral overlap integrals for each QD-dye FRET pair can be found in the SI (Figure S5, Table S6). The Förster distances for the QD630-A647 and QD650-A680 FRET pairs were 7.8 nm and 6.2 nm, respectively. Figure 4A shows that when QDs in bulk solution were assembled with increasing amounts of acceptor dye-labeled peptide substrate, Sub(A647) or Sub(A680), and energy transfer was measured in a fluorescence plate reader, the QD630-A647 pair was observed to be a more efficient FRET system. After correction for the Poisson distribution of acceptors per QD,[33] the QD630-FRET efficiency exceeded 70% with 20 acceptors per QD *versus* < 20% efficiency for the QD650-A680 (see also Figure S6). This result was consistent with the smaller Förster distance for the QD650-A680 FRET pair and the larger radius of the QD650 (~3.6 nm *versus* ~2.6 nm for QD630), which increased the effective donor-acceptor separation distance. Despite the somewhat superior brightness of the QD650, the greater FRET efficiencies associated with the QD630-A647 FRET pair and the only

somewhat better brightness of the QD650 (40% with smartphone imaging) made QD630 the preferred QD material, particularly since FRET efficiency is a key determinant of assay sensitivity. The absorption and emission spectra associated with the QD630-A647 FRET pair are shown in Figure 2.

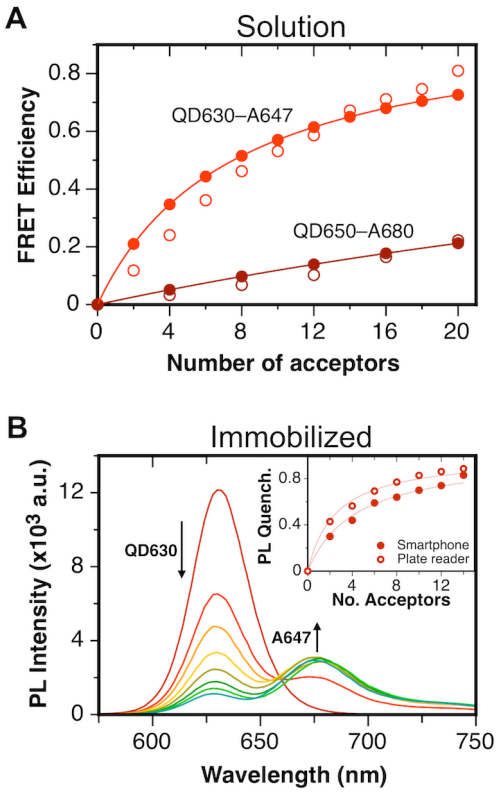

Figure 4. (A) Comparison of FRET efficiency between the QD630-A647 and QD650-A680 FRET pairs in bulk solution, measured with a fluorescence plate reader (open circles) and corrected from the Poisson distribution of acceptors per QD (closed circles). **(B)** PL spectra of paper-immobilized QD-peptide conjugates. The inset shows extent of QD PL quenching as a function of the number of acceptors, measured from spectra acquired with fluorescence plate reader (open circles) and digital images acquired with smartphone (closed circles).

Assay design: immobilization, reference spot, and PDMS sample chip

As Figure 1 illustrates, spots of substrate QD-peptide conjugates, QD630-Sub(A647), were immobilized on paper test strips alongside spots of non-substrate QD-peptide conjugates, QD630-Pep. Typical spot sizes were 2 × 2.5 mm. The spots of QD630-Sub(A647) were sensitive to thrombin activity by virtue of the LVPRGS amino acid sequence in the substrate peptide. Figure 4B shows that assembly of an average of 10 Sub(A647) acceptors per QD630 resulted in *ca*. 70% PL quenching when immobilized on the paper test strip. The same conjugates in bulk solution exhibited *ca*. 50% PL quenching, which is consistent with our previous observation of

enhanced FRET efficiencies when QDs are immobilized within a paper matrix.[34] Recovery of QD630 PL from the sample spot was expected with thrombin activity and the resultant loss of FRET. Reference spots had unquenched QD PL that was, to a first approximation, insensitive to thrombin activity. These spots were used for ratiometric data analysis to mitigate fluctuations in excitation intensity, non-uniform illumination, and variations in PL collection efficiency. Sample spots contained 20 pmol of QD630 and 200 pmol of Sub(A647), whereas reference spots contained 5 pmol of QD630 and 100 pmol of Pep. The difference in the amount of QD630 between the sample and reference spots was necessary to ensure that QD PL intensity from both spots was within the dynamic range of digital images acquired with the smartphone (or other CMOS camera device).

In the case of blood samples, and despite our efforts to optimize the selection of QDs, the biggest determinant of the observed QD PL signal was the path length through the blood. The maximum signal was observed for a path length of 250–300 μm, which was the shortest length we could control and also the most relevant to the assay format because paper test strips had a thickness of *ca*. 200 μm. For path lengths of 1.2 mm and 450 μm, 80% and 50% reductions of QD630 PL, respectively, were observed relative to the shortest path length (see Figure S8). Given the foregoing, we placed the paper test strips within 4 × 9 × 0.25 mm PDMS cells (see Figure 1B) on a glass chip. Each cell required only 12 μL of sample, minimized drying of the sample during analysis, and ensured a reproducibly short path length (*ca*. 250 μm). This format was suitable for the analysis of buffer, serum, 50% blood, and whole blood samples.

Assay design: readout platform

An array of 5 mm (T-1 ¾) LEDs was chosen to illuminate the sample chip and excite QD PL because of the compact size, low-cost, low-power requirements, and relatively wide illumination area of LEDs. To select the optimum LED for assays in whole blood, we evaluated a variety of LED types and colors that were potentially suitable for excitation of QD630 (peak emission wavelengths within the range from *ca*. 385–585 nm; see Table S7). Important considerations included the brightness of an LED, the molar absorption coefficient of the QD630 and the optical density of blood at the LED emission wavelength, and crosstalk between the long-wavelength tail of the LED emission and the QD630 PL. From the standpoint of the QD630, UV (385 nm)

and violet (405 nm) LEDs were ideal because these wavelengths corresponded to the highest molar absorption coefficients, were spectrally well-separated from the QD630 emission, and had been used effectively in previous studies with QDs.[21, 34] Unfortunately, it is in this spectral region that serum and blood most strongly attenuated light. At longer wavelengths, yellow (565, 585 nm) and orange (605 nm) LEDs were found to have relatively low brightness that, when combined with the lower light absorption by the QD630 at these wavelengths, were poorly suited for measurements. Moreover, a significant issue was very large crosstalk with the QD630 PL from the red tail of the LED emission. Blue (470 nm) and green (500, 510, 525 nm) LEDs were found to be a good compromise between maximizing excitation of the QDs and maximizing transmission through blood samples, and were available with very bright emission. A blue LED (LED470) was ultimately found to be optimum because green LEDs had significantly greater crosstalk with QD630 PL, less efficient excitation of the QD630, and lower brightness (see Table S7). The emission spectrum of the LED470 is shown in Figure 2 relative to the absorption spectrum of blood, as well as the absorption and emission spectra of the QD630.

To detect QD630 PL, either (i) a smartphone (iPhone 5S) camera or (ii) a compact, monochrome USB-CMOS camera was used. A trans-illumination configuration was adopted for excitation and readout of QD PL with the LEDs and smartphone (or USB-CMOS camera), as shown in Figure 1 (or Figure S3). When compared to an epi-illumination configuration, the trans-illumination configuration had a lower stray light and scattering background with blood samples. The open space between the sample chip and detector was also more convenient for adding samples to the chip and running assays. Pulsed LED illumination was synched with image acquisition and used to minimize effects such as photobrightening of the QD630 and photobleaching of the A647, which were observed with time under continuous illumination.

Thrombin assays

Samples containing various activities of thrombin (7.6–480 NIH units mL^{-1}) were added to cells in the sample chip, where each cell contained a paper test strip with substrate and reference spots of QD-peptide conjugates. Changes in QD630 PL were monitored over time with either smartphone or USB-CMOS camera imaging. Buffer, serum and blood samples were tested. Mean spot intensities from reference and sample spots, measured *via* images, were used to

calculate a signal ratio (see SI, Eqn. S5) that helped account for fluctuations and differences in illumination intensity between sample cells in the chip. A blank sample (*i.e.* sample and reference spot exposed to sample matrix only) was measured in parallel and used to normalize data (Eqn. S6) to account for non-proteolytic changes (see Figure S10 for examples of raw data). Smartphone imaging-derived progress curves for the digestion of Sub(A647) by increasing activities of thrombin are shown in Figure 5 as a function of the normalized QD PL intensity. The progress curves were reduced to average hydrolysis rates for quantitative analysis (see SI for details). Some adjustment of acquisition parameters (*e.g.*, LED intensity, camera exposure; see Table S4) was necessary for assaying different sample matrices. The average rates obtained from progress curves were used for quantification of thrombin in the sample. For smartphone readout, Figure 5, the limit of detection (defined as three standard deviations above the average rate calculated for progress curves for negative controls samples) was *ca.* 12 NIH units mL^{-1} for thrombin in buffer and serum, and *ca.* 18 NIH units mL^{-1} for whole blood assays. Assays with the USB-CMOS camera readout yielded results that were similar to analogous assays with smartphone readout (see Figure S11). A set of blind assays was also done to confirm that calibrations of the type in Figure 5 (and Figure S11) could be used to determine unknown thrombin activities. Table 1 summarizes these results and, within the experimental uncertainty, shows good agreement between spiked thrombin activities (unknown to the assayer) and those determined from QD PL measurements and calibration data. Notably, the precision and accuracy decrease as the thrombin activity increases and the rate of hydrolysis of Sub(A647) increases; however, this limitation is common to all rate-based enzymatic activity assays and is not unique to the readout format.

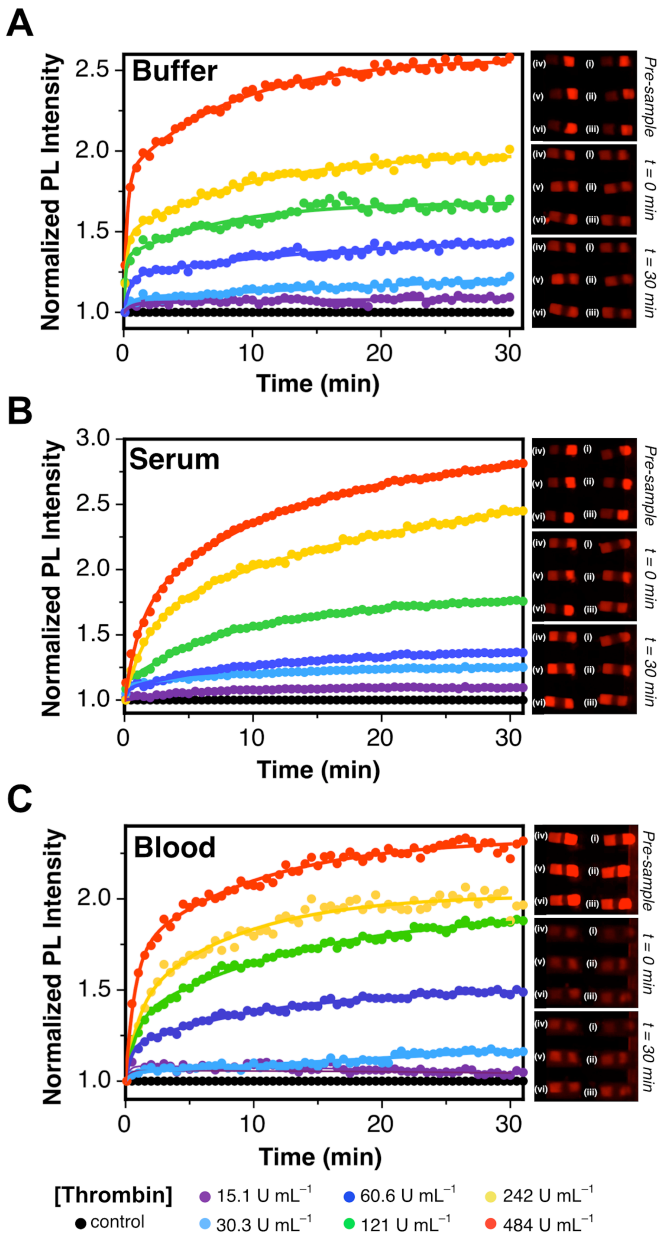

Figure 5. Normalized progress curves for thrombin activity in (A) buffer, (B) serum, and (C) whole blood samples, measured *via* smartphone imaging. Representative smartphone images are shown for three points in the assays: prior to the addition of sample, immediately after adding sample, and after 30 min. In each image, the spiked thrombin activities were (i) 0, (ii) 15.1 NIH U mL^{-1}, (iii) 30.3 NIH U mL^{-1}, (iv) 121 NIH U mL^{-1}, (v) 242 NIH U mL^{-1}, and (vi) 484 NIH U mL^{-1}.

Table 1. Results of blind assays for thrombin in whole blood.

Blind Sample	Activity of Thrombin (NIH U mL^{-1})		Relative Error (%)
	Measured	Spiked	
1	154 ± 34	157	1.9
2	96 ± 8	97	1.0
3	348 ± 85	291	20

Competitive binding assays

While activity-based assays for thrombin are analytically important,[35, 36] there are many other prospective protein analytes in blood, many of which are not hydrolase enzymes. We therefore tested a competitive binding assay format using the biotin-streptavidin interaction as a model system. As shown in the ESI (Figure S13), detection of streptavidin in 50% blood was possible at levels between 200 nM–10 μM. It should be possible to use this assay format with other more interesting protein analytes by substituting biotin with ligands for those proteins. Although preliminary, these results suggest that that QD-FRET signaling and LED/smartphone readout have the potential for broader applicability than hydrolase assays.

Discussion

There is a need for assay methods that can be applied directly in serum and, more ideally, whole blood, particularly in the context of point-of-care diagnostics. Among other criteria, these point-of-care diagnostics require simple and accessible platforms for readout of assays.[37, 38] Smartphones are highly promising candidates for assay readout because of their multitude of features, including high-quality built-in cameras, excellent storage capacity, wireless communication (LTE, WiFi, Bluetooth), and software applications (apps). Importantly, smartphones are also ubiquitous with more than 61% of mobile subscribers owning smartphones in the US (with similar ownership statistics in Canada and Europe).[39] Smartphone imaging can also generate quantitative data from diagnostic tests that have typically been qualitative (*e.g.*, colorimetric assays). Here, we have shown that careful integration of quantum dots with

smartphone imaging can offer direct, single-step and quantitative fluorescence-based detection of analytes in whole blood, in a manner that is very amenable to point-of-care applications.

Two of the major challenges faced in this work were the physical and chemical properties of whole blood. Physically, blood is a strongly absorbing, strongly scattering and autofluorescent sample matrix, often resulting in poor sensitivity in optical assays. Oxy-hemoglobin has absorption peaks centered at 541 and 577 nm, deoxyhemoglobin has an absorption peak at 555 nm, and both have strong UV absorption.[40, 41] NAD(P)H, vitamins A and B6, collagens, folic acid, and cholecalciferol fluoresce in the 300–450 nm region, and porphyrins fluoresce at 500 nm and 630 nm.[40] Blood cells are also good light scatterers.[42] Given these optical interferences, bright fluorophores with emission in the red or NIR region of the spectrum are typically used for measurement of blood and tissue specimens.[43, 44] Although, NIR wavelengths are most common and best suited to these measurements, this utility must be balanced against technical requirements in the context of prospective point-of-care diagnostics. Mass produced consumer smartphones are an ideal platform for measurements; however, their built-in IR filters preclude measurement of NIR fluorescence without custom modifications. It was for this reason that we evaluated the utility of red-emitting QDs with emission maxima centered at 630 and 650 nm rather than NIR QDs. The advantages of using QDs for smartphone-based fluorescence measurements include (i) their excellent brightness, which is better than that of most fluorescent dyes; (ii) the ability to tune their narrow emission spectra to align with the transmission bands of the built-in color filters of CMOS camera chips; and (iii) their broad absorption spectra, which can afford excellent spectral separation between excitation and emission and permit the use of light sources such as LEDs without problematic crosstalk.

Chemically, blood is a very complex sample matrix with relatively high ionic strength, a high concentration of proteins, and a multitude of small molecules. These components all have the potential to affect the properties of nanoparticles or compromise their colloidal stability. Immobilization of QDs on a paper substrate or “test strip” avoids problems with colloidal stability because the QDs are physically prevented from aggregating. Another potential challenge with blood samples is the non-specific adsorption of albumin, other proteins, cells, and other biological materials on the surface of the immobilized QDs. In this work, it appears that

immobilization of the QDs, in combination with a glutathione ligand coating and self-assembled peptides, mitigated non-specific adsorption to a degree that proteolysis (or biotin-streptavidin binding) remained possible. The immobilization format is also better suited for storage than QDs in bulk solution. Shelf life is an important consideration for prospective point-of-care use, and future work will need to address the long-term stability of our assay format. Additionally, immobilization can improve signal magnitudes because the QDs remain concentrated in a defined zone and are not diluted by the addition of biological sample. Our use of paper as an immobilization substrate was also advantageous because the porous, three-dimensional network of cellulose fibers allowed for immobilization of QDs at effective densities of *ca*. 4 pmol cm^{-2}, which improves signal levels when compared to immobilization on a substrate that only accommodates a monolayer of immobilized QDs (*e.g*., glass substrates, where *ca*. 0.8 pmol cm^{-2} are immobilized).[45] This consideration is especially important when minimizing the technical requirements for readout, such as by using low-power LEDs as an excitation source and a smartphone camera for detection of emission.

The benefits of using LEDs as excitation sources are their compact size, low-cost, several choices for excitation wavelength (*i.e*. color), and a relatively large area of illumination, the latter of which permits analysis of multiple samples simultaneously (whether for multiplexing or inclusion of control samples). Although laser diodes could provide more intense and monochromatic excitation, the small illumination area is not conducive to array-based multiplexing, and both unit cost and power consumption are greater. Nonetheless, LED illumination is not without its challenges; for example, our method had to compensate for non-uniform illumination of the sample chip, as well as temporal variation in LED intensity. We previously demonstrated that the ratiometric detection of FRET in the red and green channels of smartphone images can effectively mitigate variations in excitation intensity;[21] however, the requisite green fluorescence and violet excitation are poorly suited for a sample matrix of blood. The concept of a ratiometric or referenced measurement was therefore implemented in our present study using a two-spot system: (i) a sample spot that responded to our analyte; and (ii) a reference spot that was insensitive to the presence of analyte.

While all of the considerations discussed above were important for detection in whole blood, the optical path length through the blood remained one of the most critical factors. It was this reason that we designed a disposable PDMS/glass chip with sample cells that housed paper test strips and provided a well-controlled optical path length of *ca*. 250 μm. Application of a drop of blood on test strips resulted in a much greater path length (millimeters) that significantly reduced signals. The chip and sample cells also offered greater containment of blood samples. Notably, the PDMS component was molded on a machined template and did not require lithographic techniques or a cleanroom. All of the components of this prototype system were low-cost and either easily obtained or easily fabricated. The recent increase in the availability of low-cost, desktop 3D printing will ultimately support further optimization, refinement and manufacturing of the non-optical components of our prototype system.

Considering the assay chemistry, the QD-FRET format was advantageous because no washing step was required, and the only manipulation was to add samples to a pre-prepared chip. This capability would not be possible with colormetric assays, and most other non-QD fluorescent materials are not as suitable for integration with LED excitation and smartphone readout because of their lower brightness and small Stokes shifts. Although not all assays will be compatible with a FRET format, we have presented preliminary data that suggests a competitive assay format is viable, thus representing a potential means for the FRET detection of non-hydrolase proteins through affinity rather than activity. Another binding assay format that could also be utilized is displacement of an A647-labeled oligonucleotide from an immobilized aptamer (e.g., thrombin binding aptamer), which is a strategy that has been shown to be effective in a variety of formats.[46, 47] Moreover, a multitude of different FRET-based assays have been cataloged in the literature for a wide variety of analytes, and many of these assays will be adaptable to our platform.[9] Here, the activity of human thrombin was used as a model bloodborne analyte of biomedical importance.[35, 36] It was spiked into bovine blood samples that did not have appreciable native thrombin activity as prepared, and was useful for demonstrating that a disposable test chip, QDs and FRET could be integrated to enable single-step bioassays in whole blood, using a smartphone readout platform amenable to point-of-care diagnostic applications. The sensitivity of the assay to thrombin activity distinguishes it from other assay formats that are sensitive only to thrombin concentration (*e.g.*, lateral flow strips[48]). It should be noted, however,

that the thrombin assay does not represent the full scope of possibilities with this general assay platform, nor does it represent the best possible analytical performance that will be obtainable with further optimization.

Conclusions

We have shown that the integration of QDs, FRET and smartphone imaging with a paper-in-PDMS chip is a viable and easily accessible platform for quantitative, single-step bioassays in serum and whole blood. Although further engineering and optimization is possible, the assay format and prototype design is highly amenable to point-of-care diagnostic settings because of its portability and the use of mass-produced, low-power consumer components. The major challenge overcome in this study was the optical properties of whole blood, which imposed significant design restrictions. Our final assay design included the following components: (i) a QD630-A647 FRET pair, which achieved a compromise between transmission of QD PL through blood and FRET-based signal changes upon proteolysis; (ii) a paper test strip with reference and sample spots of QDs, which permitted localization of PL signals and ratiometric measurements; (iii) a disposable PDMS/glass sample chip, which controlled the optical path length through blood and facilitated multiplexing; and (iv) an LED470 excitation source that balanced brightness, transmission through blood, and minimization of crosstalk with QD630 PL. The successful integration of these components was demonstrated with QD-FRET assays for thrombin activity in 12 μL of serum and whole blood, with detection limits of 12 and 18 NIH units mL^{-1}, respectively. The assay platform will also be applicable with the wide range of QD-FRET methods available for the detection other analytes, as demonstrated through a mock competitive binding assay. Overall, the optical properties of QDs provide new opportunities for future point-of-care diagnostics by permitting single-step, FRET-based assays in serum and whole blood with smartphone readout.

Acknowledgements

We thank Miao Wu for assistance with blind assays. EP is grateful to the Natural Sciences and Engineering Research Council of Canada (NSERC) for a postgraduate scholarship. The authors

thank the Canada Foundation for Innovation (CFI), BCKDF, and NSERC for support of this research. WRA is also grateful for a Canada Research Chair (Tier 2) and a Michael Smith Foundation for Health Research Scholar Award.

Electronic supplementary information available: Detailed experimental methods including materials, instrumentation, data acquisition and analysis, additional results including LED characterization, QD PL spectra, spectral overlap for FRET, evaluation of the effect of blood path length on the QD PL signal, representative raw data for smartphone camera assays, representative thrombin progress curves from CMOS monochrome camera images, and data from competitive streptavidin assays with smartphone imaging.

References

1. H. Mattoussi, G. Palui and H. B. Na, *Adv. Drug Delivery Rev.*, 2012, **64**, 138-166.
2. P. Zrazhevskiy, M. Sena and X. H. Gao, *Chem. Soc. Rev.*, 2010, **39**, 4326-4354.
3. E. Petryayeva, W. R. Algar and I. L. Medintz, *Appl. Spectrosc.*, 2013, **67**, 215-252.
4. Z. Jin and N. Hildebrandt, *Trends Biotechnol.*, 2012, **30**, 394-403.
5. V. Biju, T. Itoh and M. Ishikawa, *Chem. Soc. Rev.* 2010, **39**, 3031-3056.
6. S. J. Rosenthal, J. C. Chang, O. Kovtun, J. R. McBride and I. D. Tomlinson, *Chem Biol*, 2011, **18**, 10-24.
7. E. Petryayeva, W. R. Algar and I. L. Medintz, *Appl. Spectrosc.*, 2013, **67**, 215-252.
8. J. B. Delehanty, K. Susumu, R. L. Manthe, W. R. Algar and I. L. Medintz, *Anal. Chim. Acta*, 2012, **750**, 63-81.
9. W. R. Algar, A. J. Tavares and U. J. Krull, *Anal. Chim. Acta*, 2010, **673**, 1-25.
10. S. S. Agasti, S. Rana, M. H. Park, C. K. Kim, C. C. You and V. M. Rotello, *Adv. Drug Deliver. Rev.*, 2010, **62**, 316-328.
11. R. Freeman and I. Willner, *Chem. Soc. Rev.*, 2012, **41**, 4067-4085.
12. N. Hildebrandt, K. D. Wegner and W. R. Algar, *Coord. Chem. Rev.*, 2014, **273**, 125-138.
13. W. R. Algar, H. Kim, I. L. Medintz and N. Hildebrandt, *Coord. Chem. Rev.*, 2014, **263**, 65-85.
14. H. Yu, Y. Tan and B. T. Cunningham, *Anal. Chem.*, 2014, **86**, 8805-8813.
15. Q. Wei, H. Qi, W. Luo, D. Tseng, S. J. Ki, Z. Wan, Z. Göröcs, L. A. Bentolila, T. T. Wu, R. Sun and A. Ozcan, *ACS Nano*, 2013, **7**, 9147-9155.
16. A. Roda, E. Michelini, L. Cevenini, D. Calabria, M. M. Calabretta and P. Simoni, *Anal. Chem.*, 2014, **86**, 7299-7304.
17. Q. S. Wei, W. Luo, S. Chiang, T. Kappel, C. Mejia, D. Tseng, R. Y. L. Chan, E. Yan, H. F. Qi, F. Shabbir, H. Ozkan, S. Feng and A. Ozcan, *ACS Nano*, 2014, **8**, 12725-12733.
18. H. Zhu, S. O. Isikman, O. Mudanyali, A. Greenbaum and A. Ozcan, *Lab on a Chip*, 2013, **13**, 51-67.
19. H. Zhu, U. Sikora and A. Ozcan, *Analyst*, 2012, **137**, 2541-2544.

20. E. Petryayeva and W. R. Algar, *Anal. Chem.* 2014, **86**, 3195-3202.
21. E. Petryayeva and W. R. Algar, *Anal. Chem.*, 2013, **85**, 8817-8825.
22. K. D. Wegner, Z. W. Jin, S. Linden, T. L. Jennings and N. Hildebrandt, *ACS Nano*, 2013, **7**, 7411-7419.
23. K. D. Wegner, S. Linden, Z. W. Jin, T. L. Jennings, R. el Khoulati, P. M. van Bergen en Henegouwen and N. Hildebrandt, *Small*, 2014, **10**, 734-740.
24. D. Liu, F. Wu, C. Zhou, H. Shen, H. Yuan, Z. Du, L. Ma and L. S. Li, *Sens. Actuators B*, 2013, **186**, 235-243.
25. X. Yu, H. S. Xia, Z. D. Sun, Y. Lin, K. Wang, J. Yu, H. Tang, D. W. Pang and Z. L. Zhang, *Biosens. Bioelectron.*, 2013, **4**, 129-136.
26. M. Hu, J. Yan, Y. He, H. T. Lu, L. X. Weng, S. P. Song, C. H. Fan and L. H. Wang, *ACS Nano*, 2010, **4**, 488-494.
27. J. V. Jokerst, A. Raamanathan, N. Christodoulides, P. N. Floriano, A. A. Pollard, G. W. Simmons, J. Wong, C. Gage, W. B. Furmaga, S. W. Redding and J. T. McDevitt, *Biosens. Bioelectron.*, 2009, **24**, 3622-3629.
28. S. R. Coughlin, *Nature*, 2000, **407**, 258-264.
29. J. J. Li, Y. A. Wang, W. Z. Guo, J. C. Keay, T. D. Mishima, M. B. Johnson and X. G. Peng, *J. Am. Chem. Soc.*, 2003, **125**, 12567-12575.
30. W. W. Yu and X. Peng, *Angew. Chem. Int. Ed.*, 2002, **41**, 2368-2371.
31. W. R. Algar, J. B. Blanco-Canosa, R. L. Manthe, K. Susumu, M. H. Stewart, P. E. Dawson and I. L. Medintz, *Meth. Mol. Biol.*, 2013, **1025**, 47-73.
32. A. D. Edelstein, M. A. Tsuchida, N. Amodaj, H. Pinkard, R. D. Vale and N. Stuurman, *J. Biol. Meth.*, 2014, **1**, e10.
33. T. Pons, I. L. Medintz, X. Wang, D. S. English and H. Matoussi, *J. Am. Chem. Soc.*, 2006, **128**, 15324-15331.
34. H. Kim, E. Petryayeva and W. R. Algar, *IEEE J. Sel. Top. Quantum Eletron.*, 2014, **20**, 7300211.
35. K. Y. Lin, G. A. Kwong, A. D. Warren, D. K. Wood and S. N. Bhatia, *ACS Nano*, 2013, **7**, 9001-9009.
36. M. D. Lancé, *Thrombosis J.*, 2015, **13**, 1.
37. P. Yager, G. J. Domingo and J. Gerdes, *Annu. Rev. Biomed. Eng.*, 2008, **10**, 107-144.
38. A. W. Martinez, S. T. Phillips and G. M. Whitesides, *Anal. Chem.*, 2010, **82**, 3-10.
39. A. Dugan, American's Tech Tastes Change with Times, Gallup, Inc., January 6, 2014, http://www.gallup.com/poll/166745/americans-tech-tastes-change-times.aspx (accessed November 15, 2014).
40. C. Swanson and A. D'Andrea, *Clin. Chem.*, 2013, **59**, 641-648.
41. W. G. Zijlstra, A. Buursma and W. P. Meeuwsen-van der Roest, *Clin. Chem.*, 1991, **37**, 1633-1638.
42. D. J. Faber, M. C. G. Aalders, E. G. Mik, B. A. Hooper, M. J. C. van Gemert and T. G. van Leeuwen, *Phys. Rev. Lett.*, 2004, **93**.
43. S. Luo, E. Zhang, Y. Su, T. Cheng and C. Shi, *Biomaterials*, 2011, **32**, 7127-7138.
44. S. Gioux, H. S. Choi and J. V. Frangioni, *Molecular Imaging*, 2010, **9**, 237-255.
45. E. Petryayeva and U. J. Krull, *Langmuir*, 2012, **28**, 13943-13951.
46. B. Deng, Y. Lin, C. Wang, F. Li, Z. Wang, H. Zhang, X. F. Li and X. C. Le, *Anal. Chim. Acta*, 2014, **837**, 1-15.
47. R. Nutiu and Y. Li, *Chem. Eur. J.*, 2004, **10**, 1868-1876.

48. H. Xu, X. Mao, Q. Zeng, S. Wang, A. N. Kawde and G. Liu, *Anal. Chem.*, 2009, **15**, 669-675.